Nanostructured hard magnets

Julia Lyubina and Oliver Gutfleisch

Institute for Metallic Materials,
IFW Dresden, Germany

Outline

- Fundamental concepts
- Nd(Pr)-Fe-B alloys
- Sm-Co alloys
- Fe-Pt alloys

incl. preparation

- sintering
- hydrogen-assisted methods (HD, HDDR)
- melt spinning
- mechanical alloying
- hot deformation

A (very) brief history of permanent magnets

Μαgnεtisμ, Μαgnεts go back to ancient Greek:
magnetite (Fe_3O_4) = loadstone

China: earliest literary reference to magnetism in a
"Book of the Devil Valley Master /鬼谷子/" (4th century BC)

- spoon-shaped compass 2000 years ago
- open-sea navigation since 1175 AD

A (very) brief history of permanent magnets

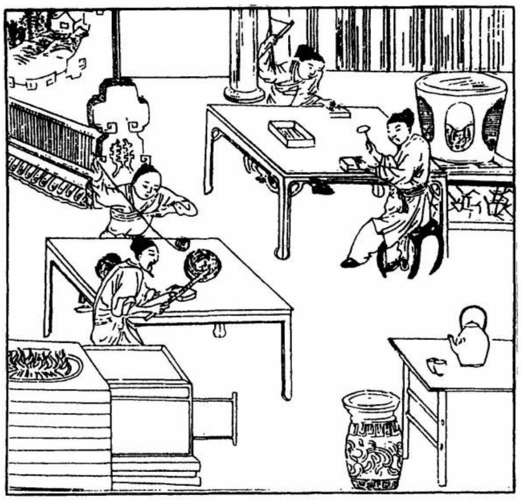

Print of 1637

The first plant in China manufacturing magnetic needles for compasses

What is a permanent magnet?

Permanent magnet/hard magnet – sample with a net magnetisation (remanence J_r)

Soft magnetic material

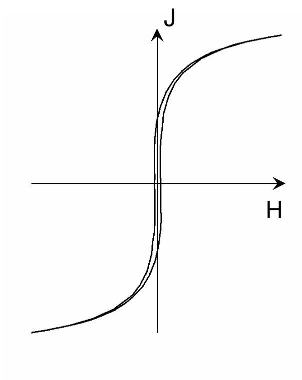

Hard magnetic material

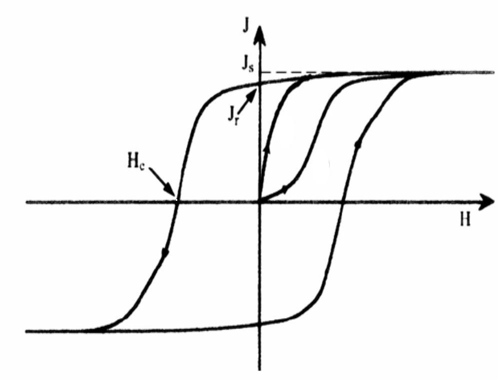

Classification based on coercivity H_c
(how easily the material can be demagnetised)

Why permanent magnets?

- Strong fields in small volumes
- Compact
- No power
- No cooling

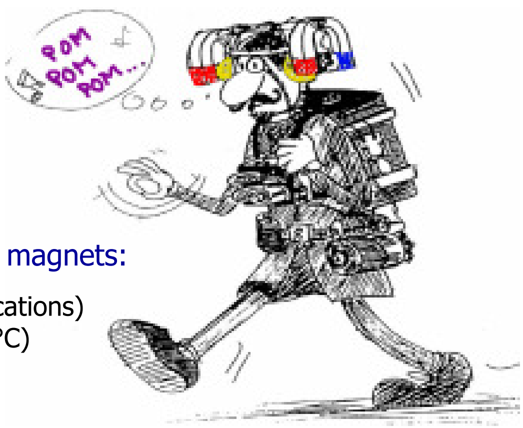

Materials for high performance magnets:

Nd-Fe-B (room temperature applications)
Sm-Co (high temp. up to ≈ 350 °C)

- brittle
- low corrosion resistance

The Walkman circa 1905

Energy product $(BH)_{max}$

Energy product $(BH)_{max}$ – magnetic energy per unit volume which can be maximally stored by a permanent magnet

$$B(H) = \mu_0 H + J = \mu_0 (H + M)$$

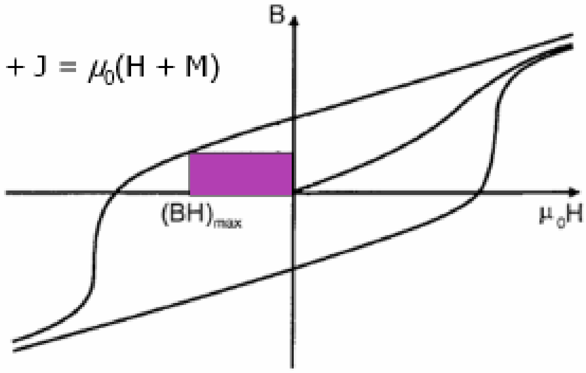

Theoretical upper limit $(BH)_{max} = (J_s)^2/4\mu_0$

Progress in the energy product

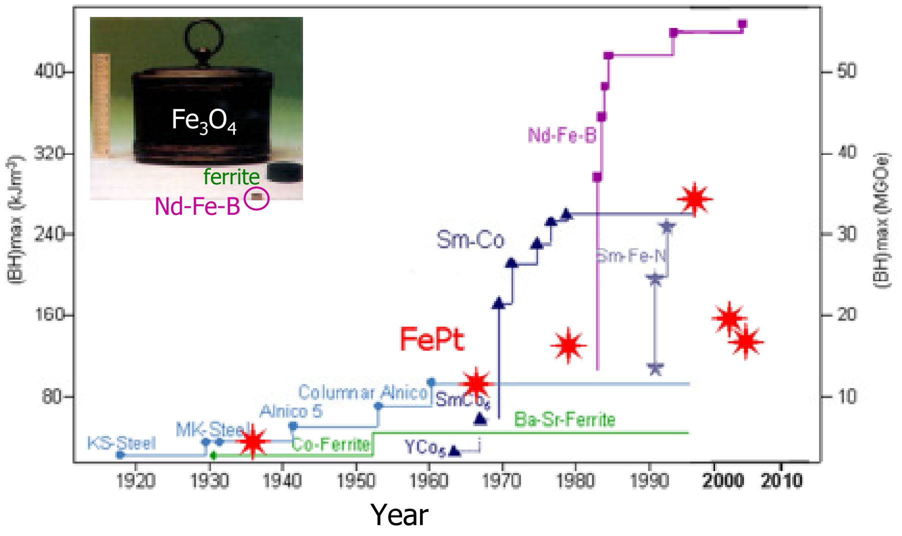

Intrinsic magnetic properties

	T_C (K)	K_1 (MJm^{-3})	$\mu_0 M_S$ (T)	
$Nd_2Fe_{14}B$	585	4.9	1.60	highest $(BH)_{max}$
$SmCo_5$	993	17	1.05	highest operating temp.
$L1_0$ FePt	750	6.6	1.43	high corrosion resistance, mechanical strength
AlNiCo	1133	0.04	1.20	high temperature stability, high corrosion resistance
$BaFe_{12}O_{19}$	720	0.3	0.47	low cost (!), good chem. stability, electrical resistance
α-Fe	1043	0.05	2.16	

Extrinsic magnetic properties

intrinsic properties + **microstructure 100 µm > D > 1 nm** = **extrinsic properties**

saturation polarisation $\mathbf{J_s}$

anisotropy field $\mathbf{H_a}$

Curie temperature $\mathbf{T_c}$

remanence $\mathbf{J_r}$

coercivity $\mathbf{H_c}$

energy density $\mathbf{(BH)_{max}}$

Critical length (nm)	$Nd_2Fe_{14}B$	α-Fe
$\delta_w = (A/K_1)^{1/2}$	3.9	30
$D_c \sim \mu_0 (A/K_1)^{1/2} / J_s^2$	214	6

$\mathbf{D_c}$: critical single-domain particle size

$\boldsymbol{\delta_w}$: domain wall width

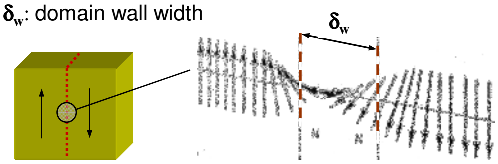

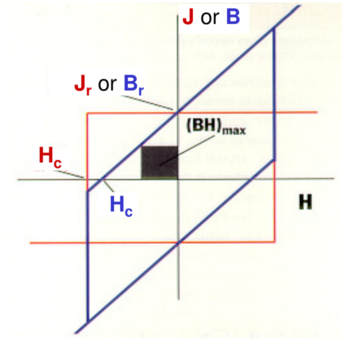

Critical lengths / definition *nanocrystalline?*

For spherical particles with uniaxial anisotropy, the critical single-domain diameter

$$[Kittel\ 1949] \quad D_c = \frac{72\sqrt{AK_1}}{\mu_0 M_s^2}$$

The competition between exchange and magnetostatic energy - exchange length (determines the grain size below which the hysteresis loops of multi-phase magnets show a single-magnetic-phase behaviour)

$$l_{ex} = \sqrt{\frac{A}{\mu_0 M_s^2}}$$

The comparison between exchange and anisotropy - wall-width parameter

$$\delta_w = \sqrt{A/K_1}$$

Understanding and optimising properties

MAGNETIC PROPs

- intrinsic ↔ extrinsic
- coercivity mechanisms
- intergrain coupling
- magnetic microstructure

NON-MAGNETIC PROPs

- grain size (μm or nm)
- texture
- hot workability
- temperature stability
- chemical stability

PROCESSING

- sintering
- melt-spinning
- mechanical alloying/milling
- HDDR
- (hot) deformation

PHASE CHARACTERISATION

- structure identification
- quantification
- (micro-) chemistry
- metastability
- transformation
- crystallographic relationships

Nd-Fe-B alloys

Phase diagram and crystal structure

Sintered magnets

Anisotropic bonded magnets (HDDR)

Hot deformed magnets

$Nd_2Fe_{14}B$ phase

Crystal structure

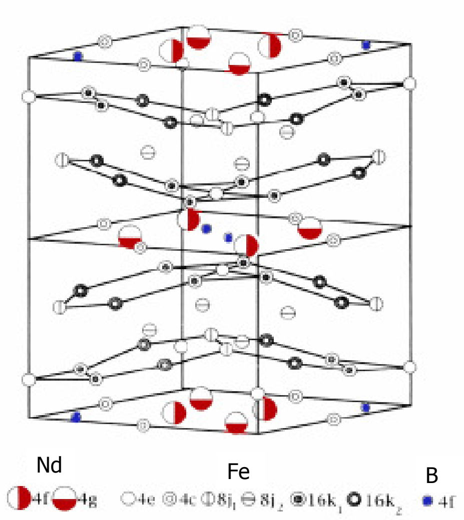

Space group: $P4_2/mnm$

68 atoms per unit cell

a = 8.8 Å; c = 12.2 Å

c-axis → easy magnetisation axis

Nd-Fe-B phase diagram (vertical sections)

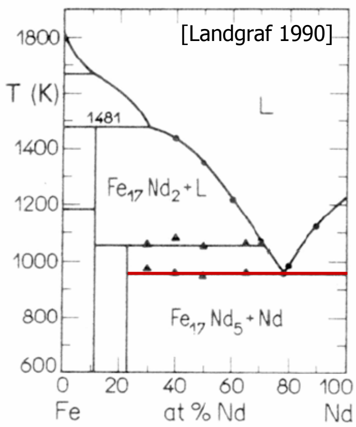

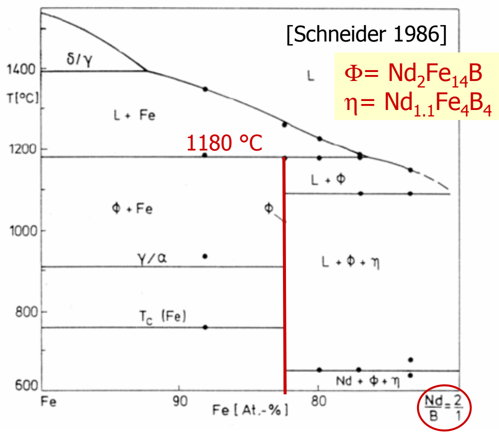

Above 685 °C → liquid phase

$Nd_2Fe_{14}B$: very narrow homogeneity range

A departure from the stoichiometry ⇒ foreign phases

Prototypes of $R_2Fe_{14}B$-based magnets

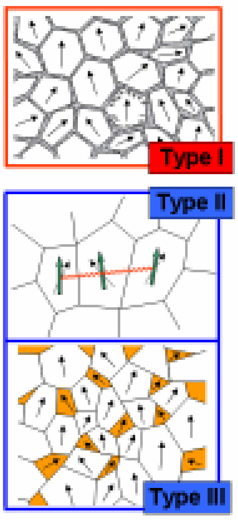

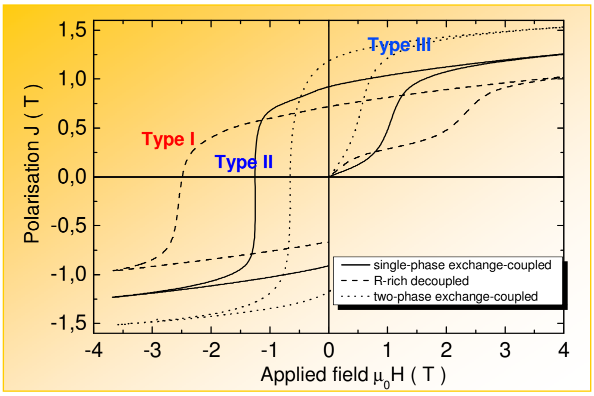

Type I: decoupled $R_2Fe_{14}B$ grains separated by thin paramagnetic layer → ↑ H_c

Type II: exchanged coupled grains based on stoichiometric $R_2Fe_{14}B$

Type III: exchanged coupled grains based on nanocomposite $R_2Fe_{14}B$ / α-Fe

(Type II and Type III) → ↑ J_r

Principal processing routes

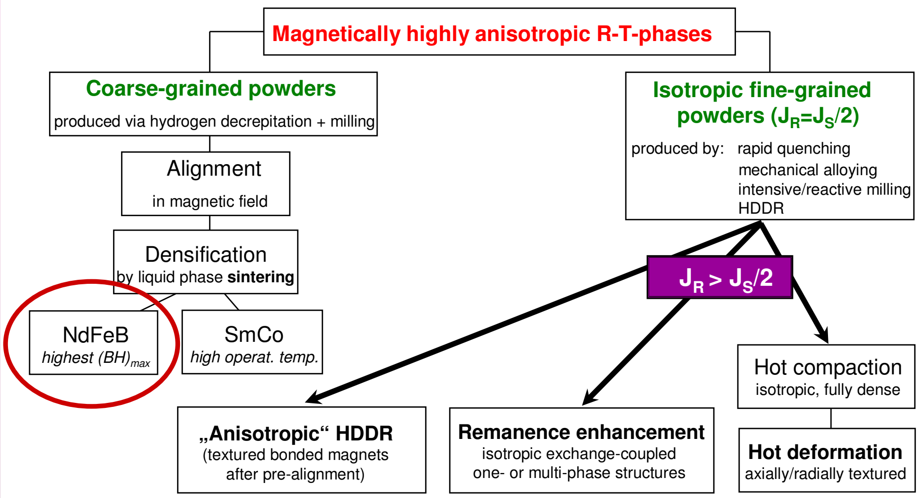

Highest $(BH)_{max}$ magnets

O. Gutfleisch, J. Phys. D: Appl. Phys. **33** (2000) R157.

Sintering

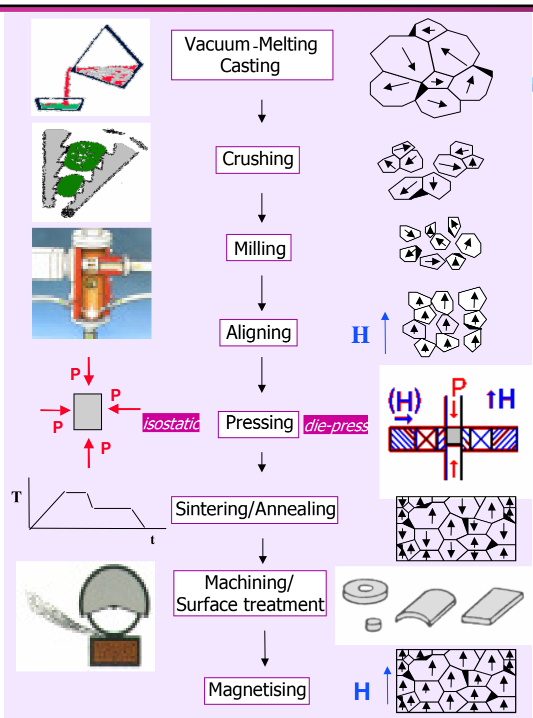

5-60 µm particles

H ~ 10 kOe

T ≈ 1000 °C

adapted from
Vacuumschmelze GmbH

Sintered Nd-Fe-B magnet

$(BH)_{max}$= 451 kJ/m³

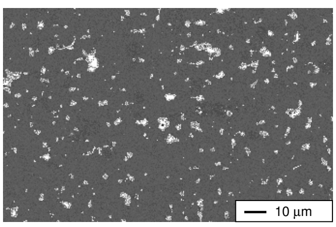

SEM
(BSE
mode)

Average grain size ~ 5 mm

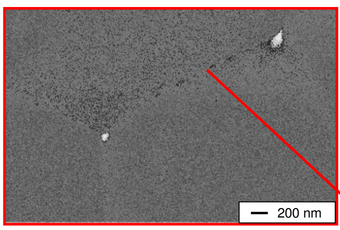

Very thin coating of 2-14-1 grains
with Nd-rich intergranular phase

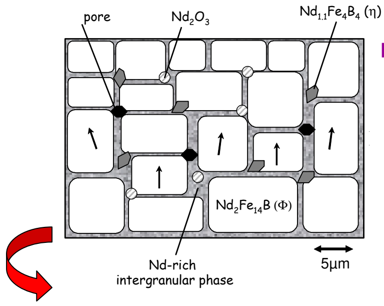

real

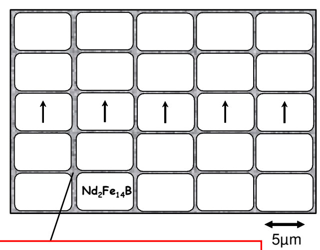

ideal

Nd-rich intergranular phase

Sintered Nd-Fe-B magnet

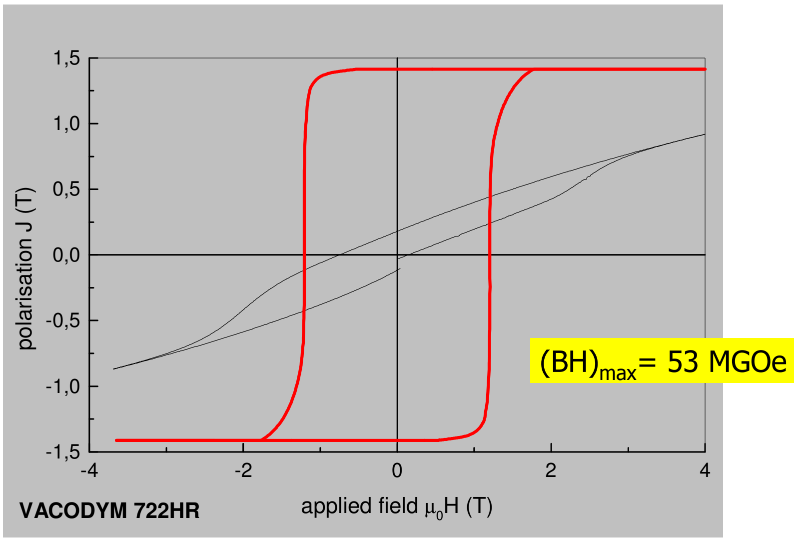

Microtexture and domain structure of anisotropic magnet

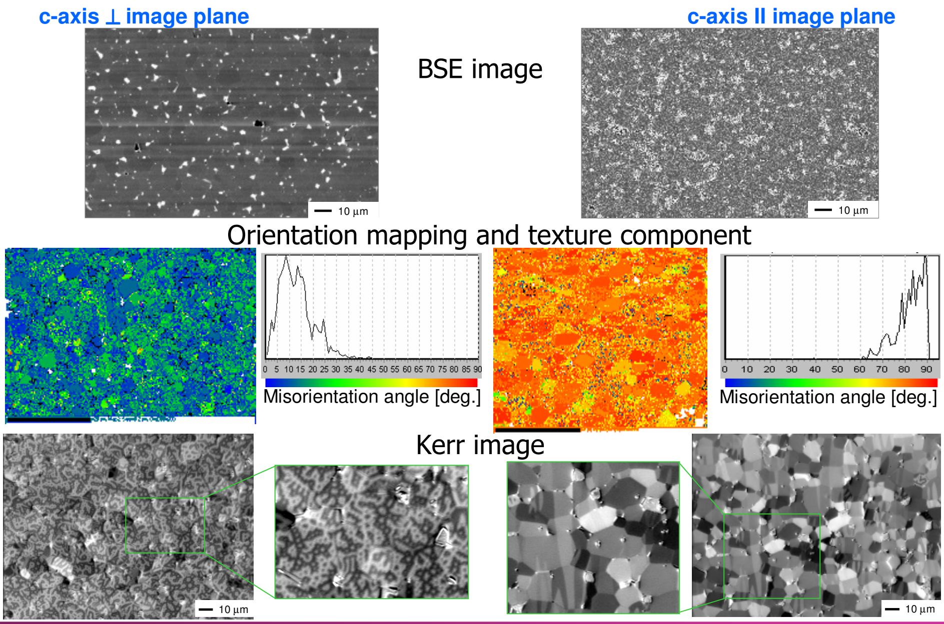

Microtexture and domain structure of isotropic magnet

Backscattered electron image

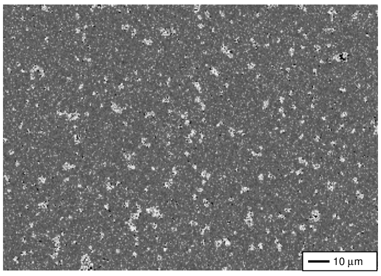

Kerr image

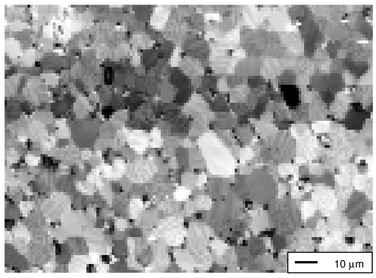

Orientation mapping and texture component

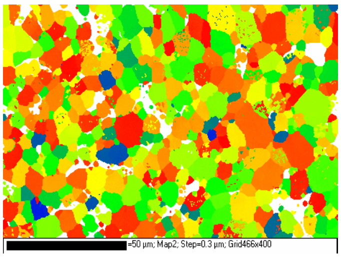

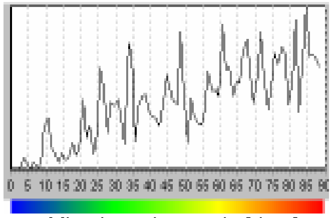

Misorientation angle [deg.]

Texture evaluation: sintered NdFeB

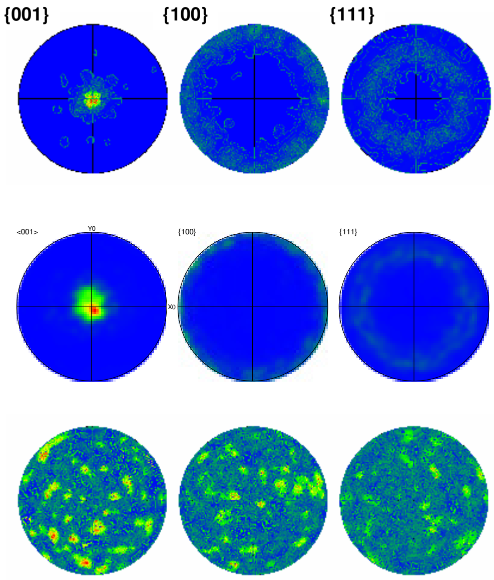

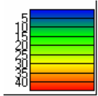

Anisotropic magnet with $(BH)_{max}$ = 56.7 MGOe

B_r = 1.52 T

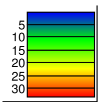

Vacodym 722 commercial grade magnet

B_r = 1.47 T

Isotropic magnet

B_r = 0.78 T

J. Alloys and Comp. 365 (2004) 259

Sintering

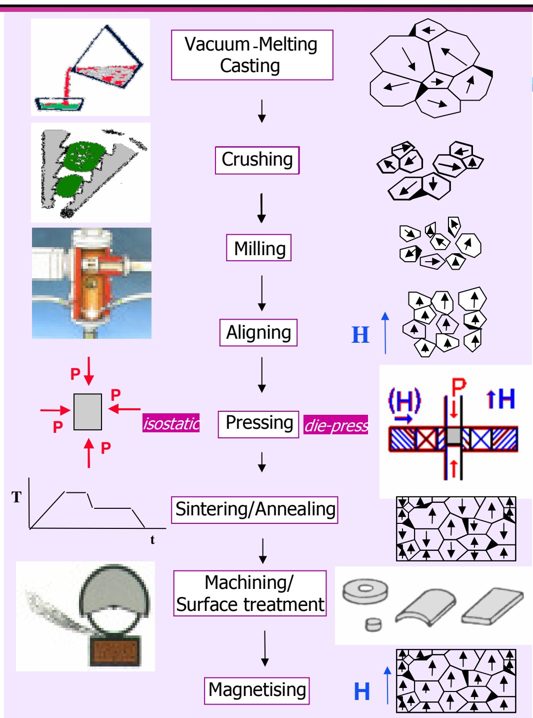

by hydrogen decrepitation

5-60 µm particles

adapted from
Vacuumschmelze GmbH

Hydrogen decrepitation (HD) process

Decrepitation → self-pulverisation of large metal particles into powder

Hydrogen decrepitation (HD) process

Crystallographic orientation

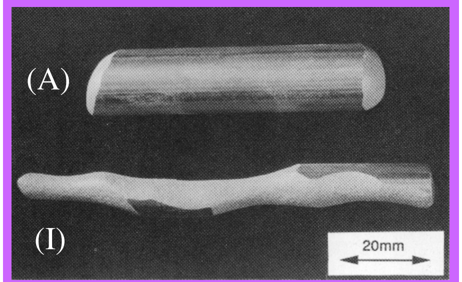

Hydrogen decrepitated anisotropic and isotropic sintered NdFeB magnets

Intergranular failure

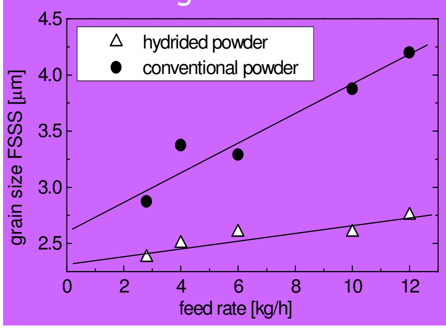

Beneficial effect of HD process on feed rate in a jet mill comparing conventional and hydrided powder

Incorporation of small amounts of H_2 into $Nd_2Fe_{14}B$!

Possible reactions of R-T compounds with H_2

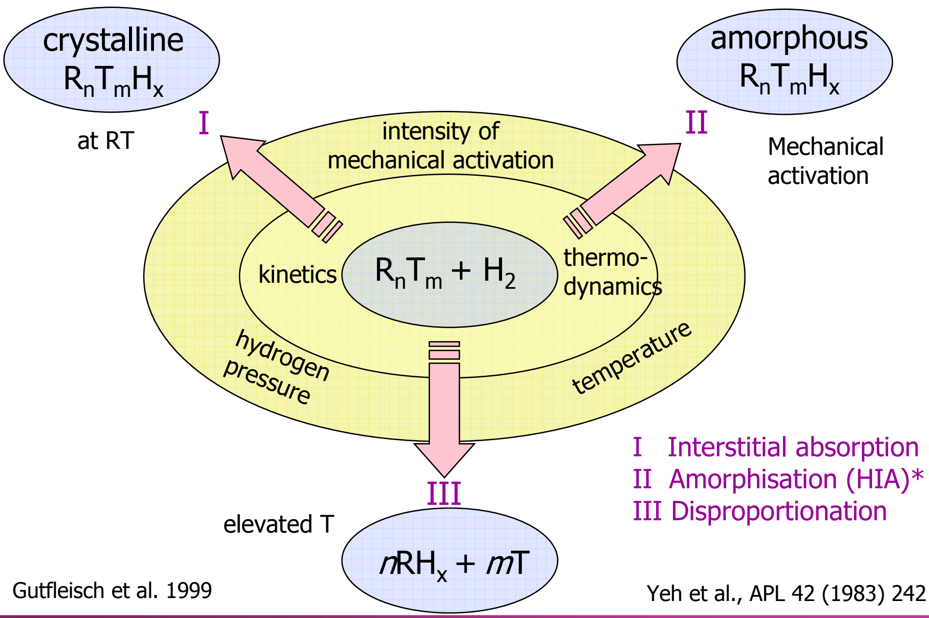

I Interstitial absorption
II Amorphisation (HIA)*
III Disproportionation

Gutfleisch et al. 1999

Yeh et al., APL 42 (1983) 242

Interstitial modification and intrinsic magnetic properties

e.g. $R_2Fe_{14}B$

H_2 uptake ⇒ change of e^- density, band structure, volume

⇓

modification of

- *3d-3d* and *3d-4f* exchange interactions
- magnetic moments
- anisotropy
- spin reorientation transition

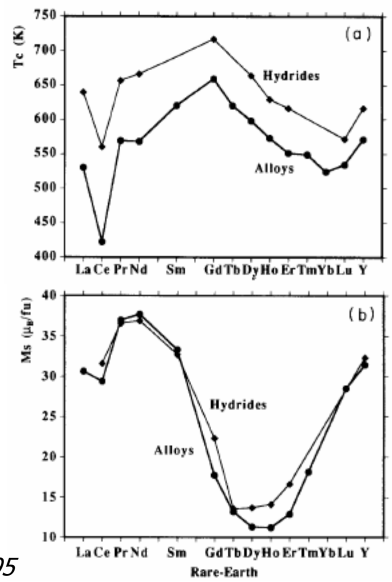

Soubeyroux et al., J. Alloys Comp. 1995

Hydrogen absorption in $Nd_2Fe_{14}B$ and Sm_2Fe_{17}

(1) Hydride formation (at moderate pressure and temperature)

(2) Hydrogen decrepitation (HD)

$$Nd_2Fe_{14}B + \tfrac{1}{2} xH_2 \Leftrightarrow Nd_2Fe_{14}BH_x \pm \Delta H_1$$

(3) Hydrogenation disproportionation desorption recombination (HDDR)

$$Nd_2Fe_{14}B + (2\pm x)H_2 \Leftrightarrow 2NdH_{2\pm x} + 12Fe + Fe_2B \pm \Delta H_2$$

$$Sm_2Fe_{17} + (2\pm x)H_2 \Leftrightarrow 2SmH_{2\pm x} + 17Fe \pm \Delta H_2^*$$

More favourable, since heat release $\Delta H_2 > \Delta H_1$

✓ Hydrogen solution is a *metastable condition*

✓ At room temperature, reaction (3) is prevented by the absence of sufficient *kinetics*

Hydrogen absorption in $Nd_2Fe_{14}B$ and Sm_2Fe_{17}

(1) Hydride formation (at moderate pressures and temperature)

(2) Hydrogen decrepitation (HD)

$$Nd_2Fe_{14}B + \tfrac{1}{2}\, xH_2 \Leftrightarrow Nd_2Fe_{14}BH_x \pm \Delta H_1$$

(3) Hydrogenation disproportionation desorption recombination (HDDR)

$$Nd_2Fe_{14}B + (2\pm x)H_2 \Leftrightarrow 2NdH_{2\pm x} + 12Fe + Fe_2B \pm \Delta H_2$$

$$Sm_2Fe_{17} + (2\pm x)H_2 \Leftrightarrow 2SmH_{2\pm x} + 17Fe \pm \Delta H_2^*$$

$\Delta H_2 > \Delta H_1$

✓ Hydrogen solution is a *metastable condition*

✓ At room temperature, reaction (3) is prevented by the absence of sufficient *kinetics*

Magnetic hardening using HDDR

Standard-HDDR (`Hydrogenation Disproportionation Desorption Recombination´)

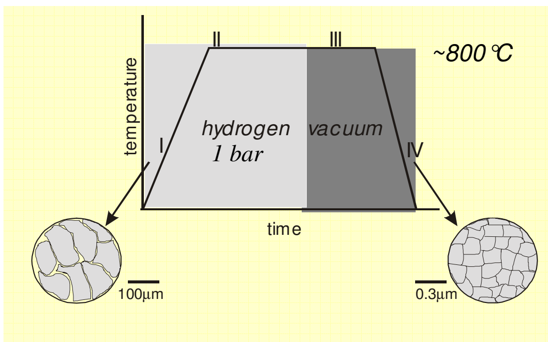

HDDR reaction:

$$Nd_2Fe_{14}B \Rightarrow NdH_x + Fe + Fe_2B \Rightarrow Nd_2Fe_{14}B$$

grain refinement via a reversible hydrogen sorption ⇒ improved coercivity

O. Gutfleisch and I.R. Harris, J. Phys. D: Appl. Phys. 29 (1996) 2255

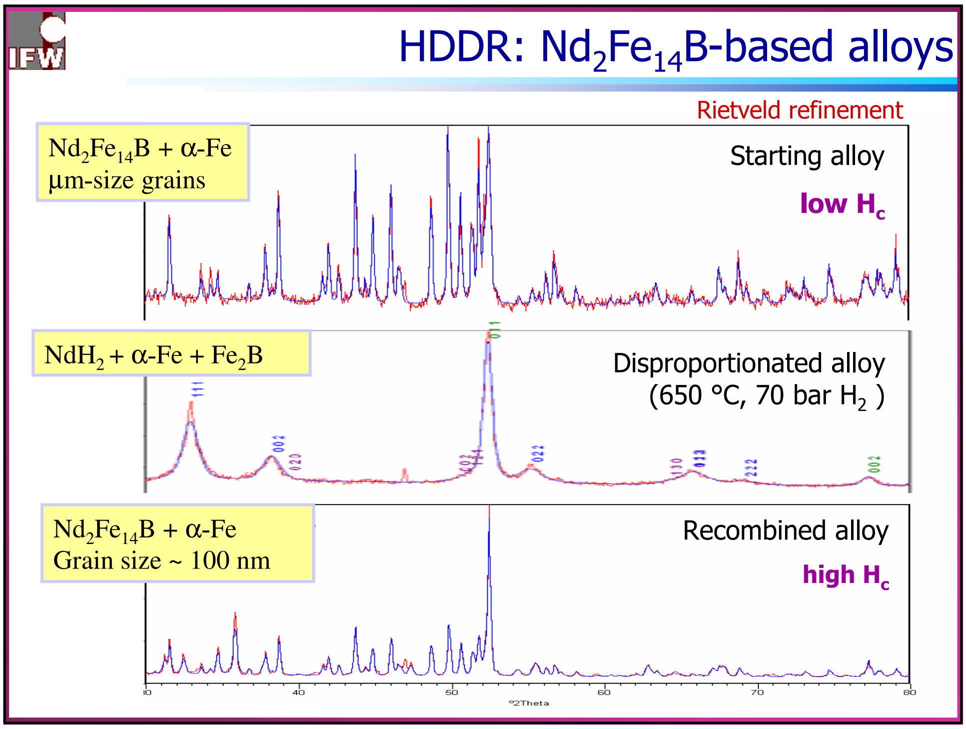

HDDR: $Nd_2Fe_{14}B$-based alloys
Rietveld refinement
$Nd_2Fe_{14}B$ + α-Fe
µm-size grains
Starting alloy
low H_c
NdH_2 + α-Fe + Fe_2B
Disproportionated alloy
(650 °C, 70 bar H_2)
$Nd_2Fe_{14}B$ + α-Fe
Grain size ~ 100 nm
Recombined alloy
high H_c

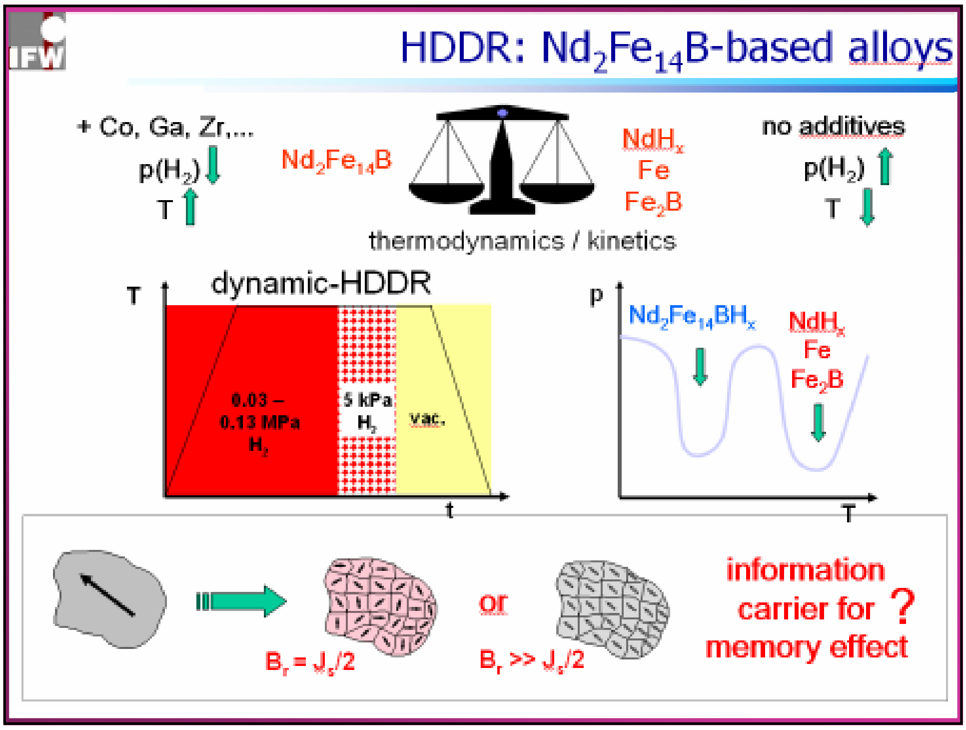

HDDR: $Nd_2Fe_{14}B$-based alloys
+ Co, Ga, Zr,...
$p(H_2)$
T
$Nd_2Fe_{14}B$
NdH_x
Fe
Fe_2B
no additives
$p(H_2)$
T
thermodynamics / kinetics
dynamic-HDDR
T
0.03 – 0.13 MPa H_2
5 kPa H_2
vac.
t
p
$Nd_2Fe_{14}BH_x$
NdH_x
Fe
Fe_2B
T
$B_r = J_s/2$
or
$B_r >> J_s/2$
information carrier for memory effect ?

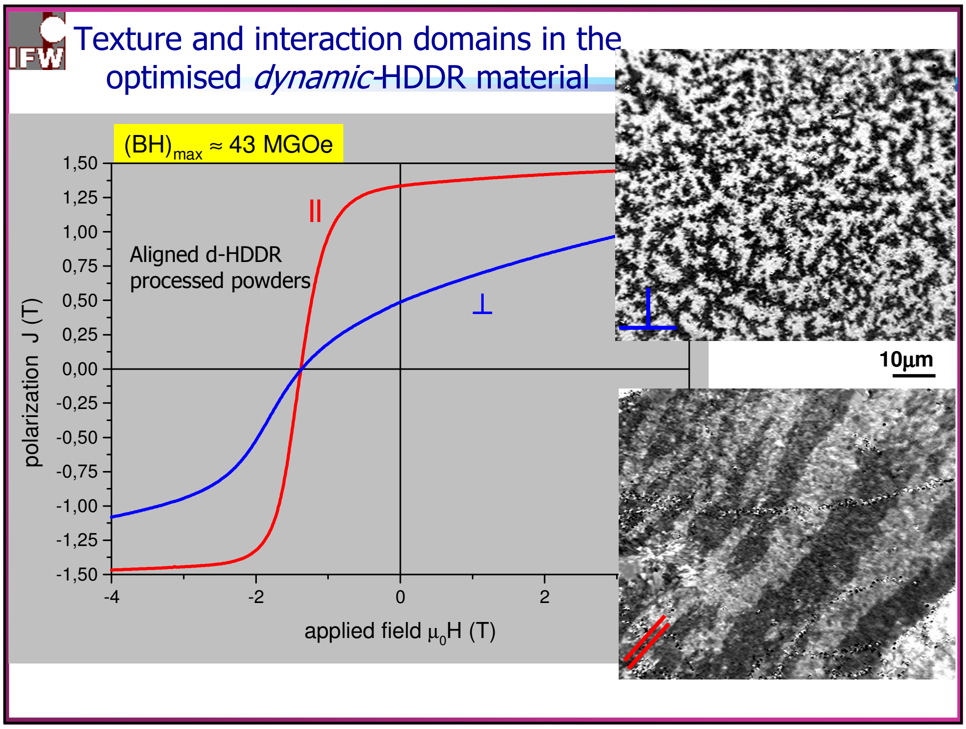
Texture and interaction domains in the optimised dynamic-HDDR material
(BH)max ≈ 43 MGOe
Aligned d-HDDR processed powders
polarization J (T)
applied field μ0H (T)
10µm

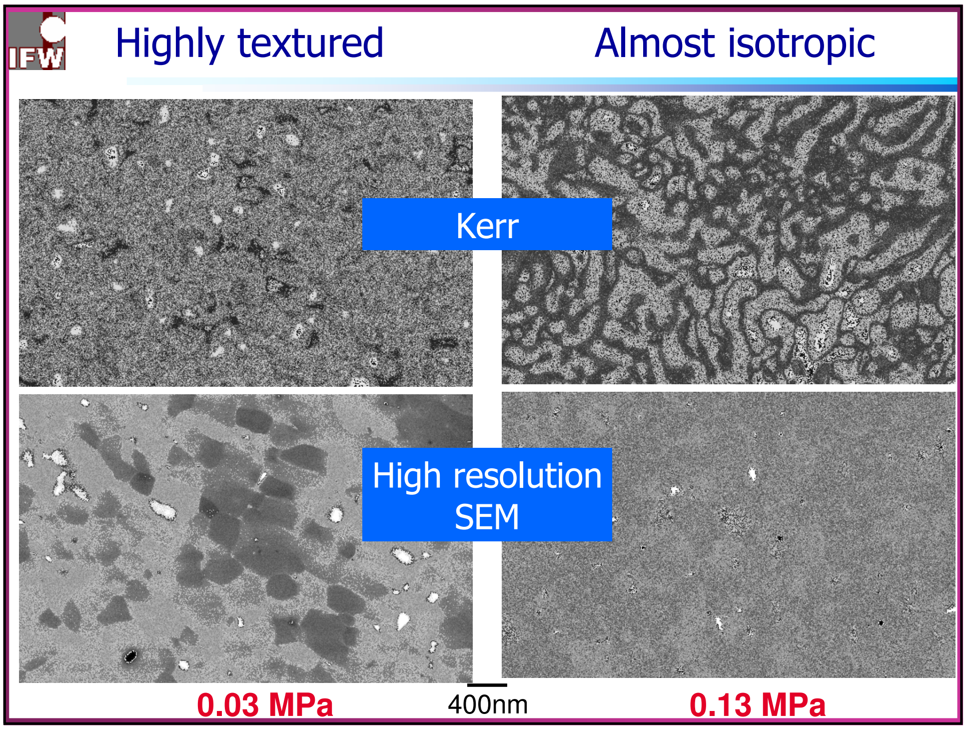
Highly textured
Almost isotropic
Kerr
High resolution SEM
0.03 MPa
400nm
0.13 MPa

Partially disproportionated state (TEM)

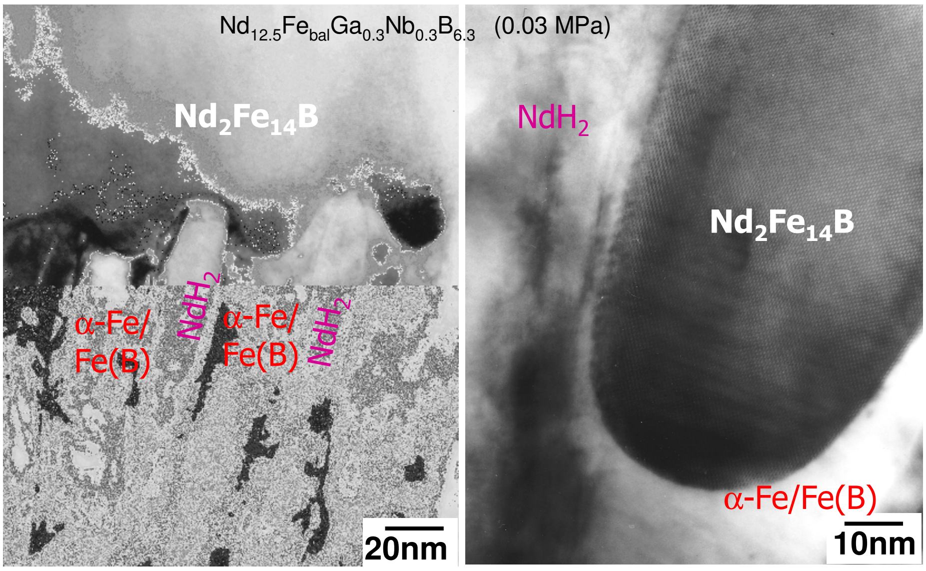

J. Magn. Magn. Mat. 290-291 part 2 (2005) 1282.

Completely disproportionated state

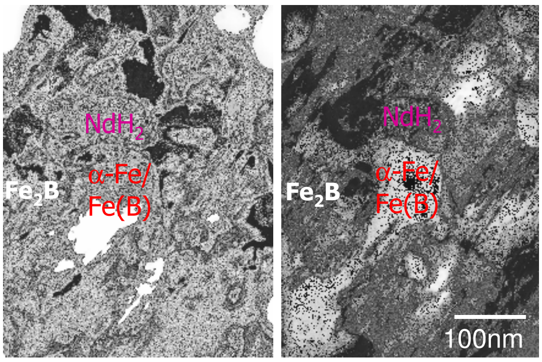

the 002 reflection of Fe_2B was used for CDF image

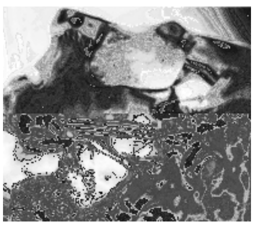

aligned Fe_2B grains !

Tetragonal Fe_2B the only reaction product with uniaxial crystal symmetry

Fe_2B at different processing stages

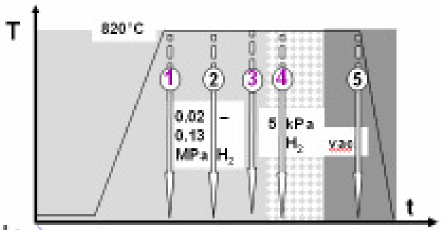

J. Magn. Magn. Mat. 290-291 part 2 (2005) 1282.

Fe_2B keeps its orientation
→ misorientation angle 20°

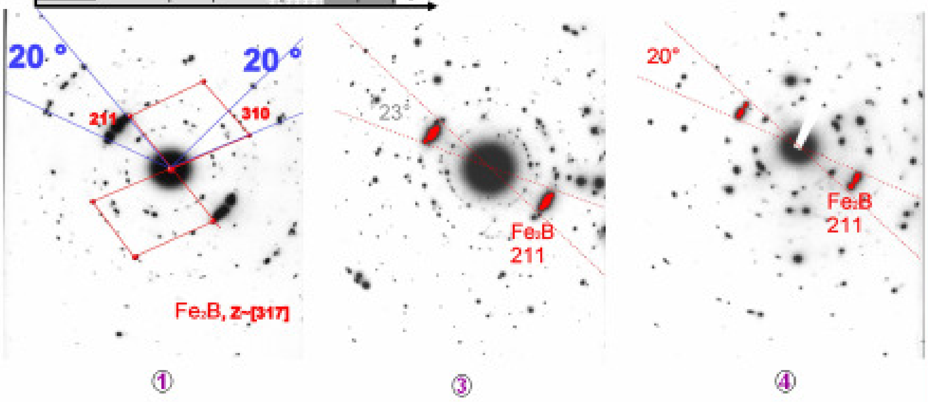

Extreme HDDR

´Standard´ HDDR (~1 bar H_2) does *NOT* work for every R-T compound

High pressure (~ 70 bar H_2) disproportionation

Stabilisation by ***additives***

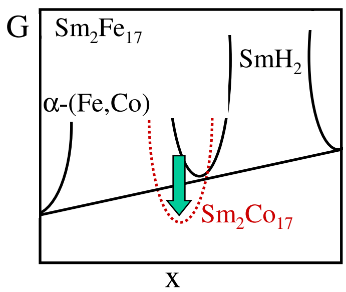

Increase of ***hydrogen pressure***

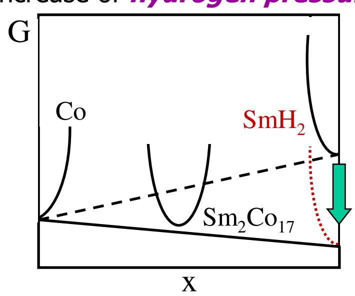

Gutfleisch et al. 1999

Can HDDR be influenced by a magn. field?

Summary: HDDR

D-HDDR

- ✓ Degree of texture depends strongly on the hydrogen pressure during the different stages
- ✓ Well-correlated Fe_2B grains could act as the anisotropy-mediating phase
- ✓ High stability of the information carrier under low hydrogen pressures makes the *d*-HDDR process applicable for the industrial production of anisotropic powders

HDDR in magnetic field

- ✓ Recombination reaction is affected by external magnetic fields
- ✓ Field processing can be used as an additional tool to tailor microstructure of hard magnetic materials

Sm-Co alloys

Phase diagram

High temperature magnets

Coercivity

Interaction domains

Principal processing routes

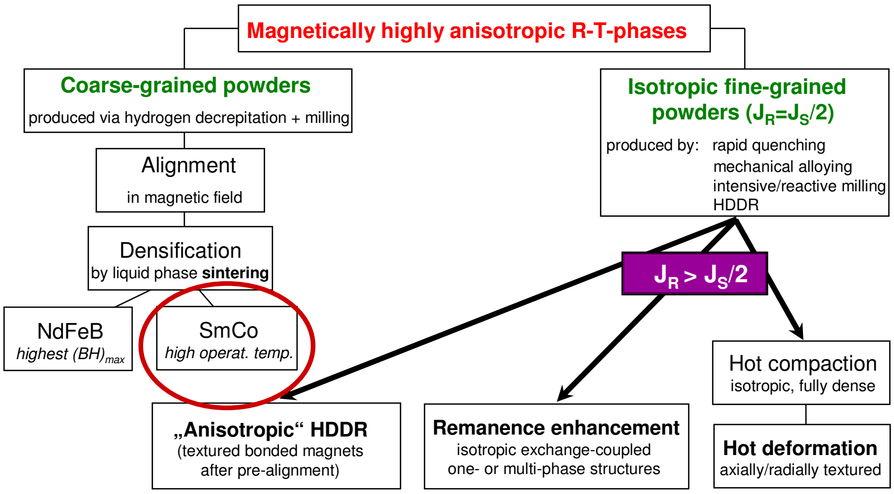

Highest operating temperatures

O. Gutfleisch, J. Phys. D: Appl. Phys. **33** (2000) R157.

Precipitation hardened magnets

Compound	Structure type	T_C (K)	$\mu_0 H_A$ (T)	$\mu_0 M_S$ (T)
$SmCo_5$	Hexagonal $CaCu_5$	993	40	1.05
Sm_2Co_{17}	Rhombohedral Th_2Zn_{17}	1100	6.5	1.30

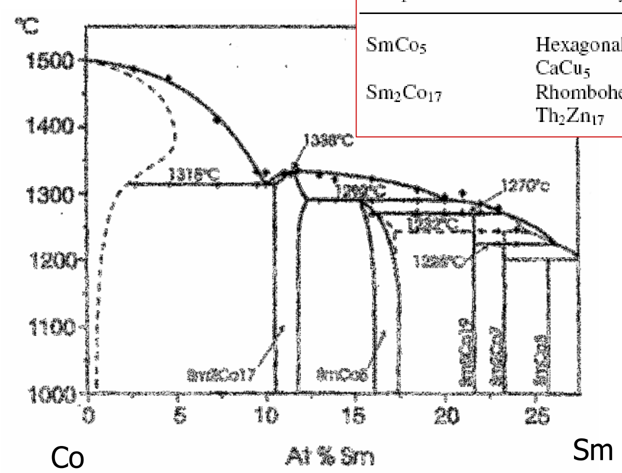

Sm-Co phase diagram (Cataldo et al. 1996).

Sm-Co system: structural transformations

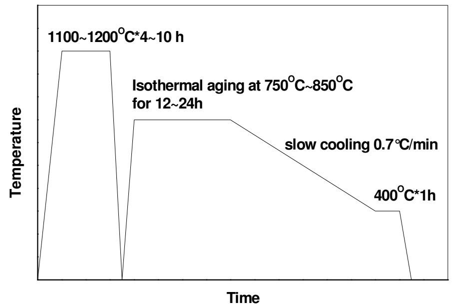

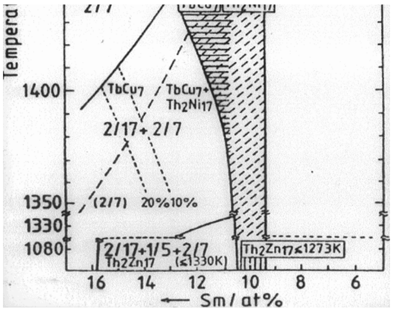

HEAT-TREATMENT		STRUCTURE
Sintering (1210-1230 °C)	→	• 2:17 H formation • Elements taken into solution • Densification
Solution treatment (1180 –1200 °C)	→	• 1:7 H formation
Quenching to RT	→	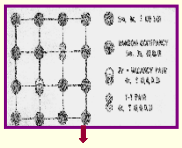
Isothermal aging (800 – 875 °C) and slow cooling (~1.0 K/min) to 400 °C	→	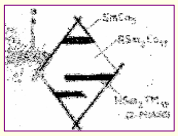

Precipitation-hardened 2:17 Sm_2Co_{17} magnets

$Sm(Co_{bal}Fe_vCu_yZr_x)_7$: typical microstructure

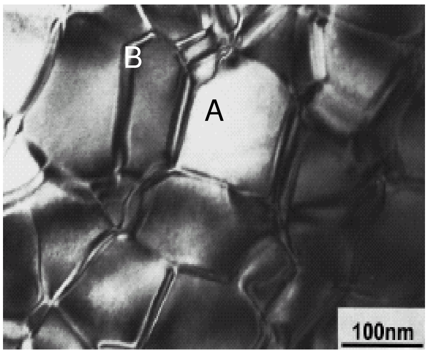

⊥ *c*

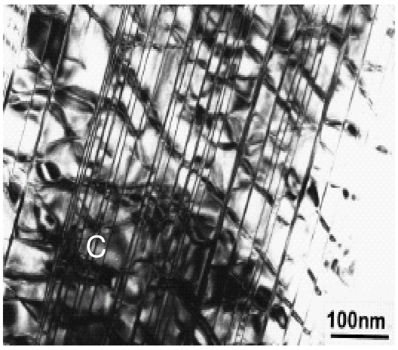

∥ *c*

A: 2:17 rhombohedral phase

B: 1:5 hexagonal (H) phase

C: lamellar phase (R B_3Nb-type)

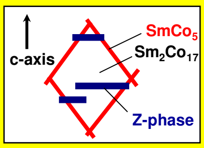

Hadjipanayis et al, 1999

2:17 SmCo: high temperature grade

$Sm(Co_{0.784}Fe_{0.1}Cu_{0.088}Zr_{0.028})_{7.19}$

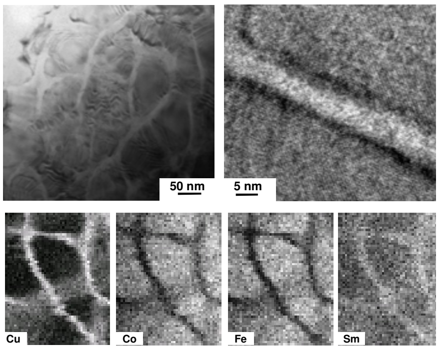

Element mapping in TEM

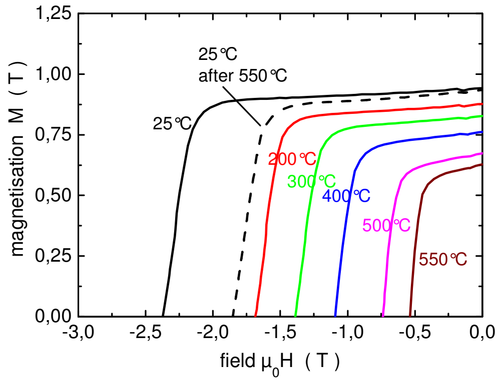

at 500 °C: $(BH)_{max}$ = 82 kJ/m³
J_r = 0.67 T
$\mu_{0i}H_c$ = 0.74 T

A. Handstein et al., IEEE Trans. on Magn. 39 (2003) 2923

2:17 SmCo: in-situ measurement at 500 °C

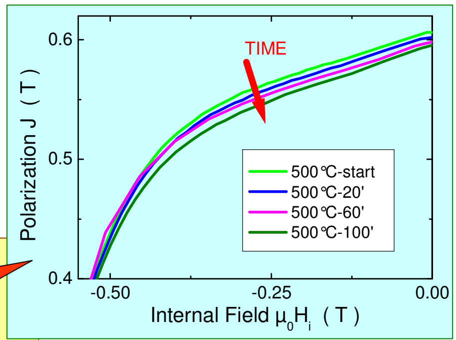

$Sm(Co_{0.738}Fe_{0.144}Cu_{0.088}Zr_{0.028})_{7.19}$

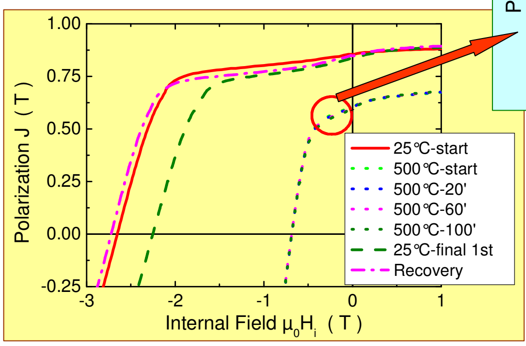

- Degradation of B_r & $(BH)_{max}$ with increasing time

! RECOVERY of ${}_jH_c$ after repetition of last segment of original heat treatment ⇒

Changes of microchemistry in 1:5-type cell boundary phase

Sm_2Co_{17} ribbons

Simple processing: no solid solution treatment
no isothermal aging at 850 °C

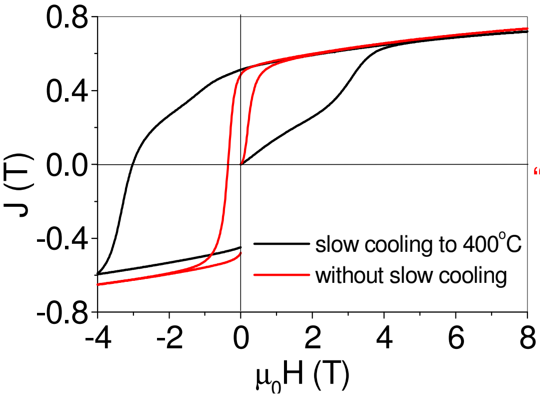

"type I" ribbon

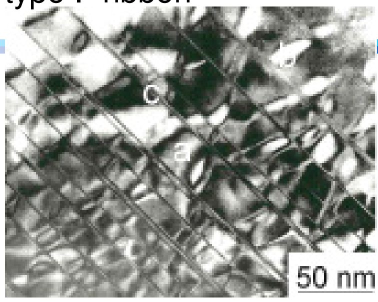

"type II" ribbon

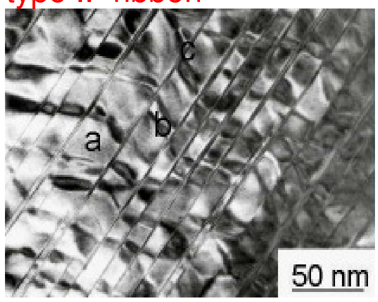

A. Yan et al., Appl. Phys. Lett. 80 (2002) 1243
A. Yan et al, IEEE Trans. Magn. 38 (2002) 2937

$Sm(Co,Fe,Cu,Zr)_{7.5}$: EDX Cu profiles near cell boundary

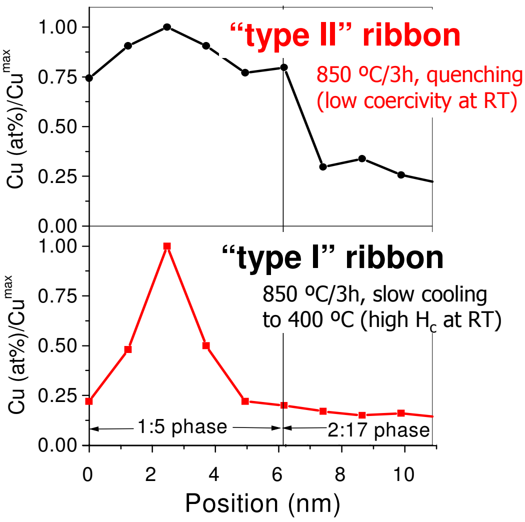

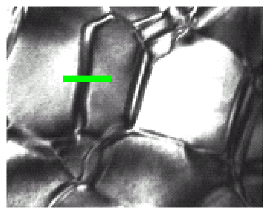

TEM

→ large gradient of Cu *within* the cell boundary phase of the highly coercive ribbons

⇓

pinning force modified

A. Yan, O. Gutfleisch, T. Gemming, K.-H. Müller, J. Appl. Phys. 93 (2003) 7975

Principal processing routes

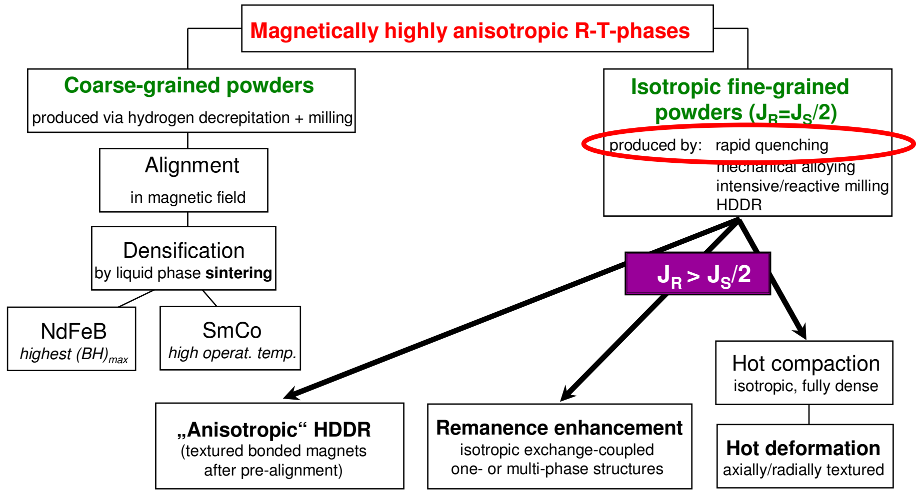

O. Gutfleisch, J. Phys. D: Appl. Phys. **33** (2000) R157.

Melt spinning

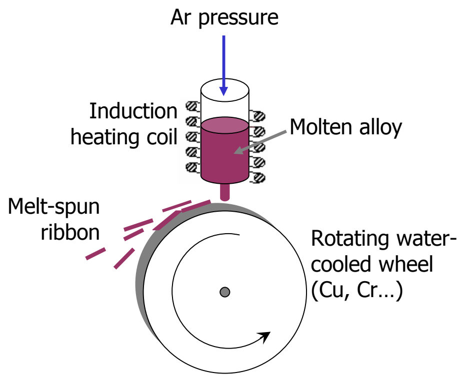

Solidification rate up to 10^5-10^6 K/s

- wheel rotation speed v_s
- type and pressure of the inert gas
- crucible opening size
- distance crucible ↔ wheel
- temperature of the melt

Melt-spun Nd-Fe-B

Underquenched (very slow v_s)
Optimally quenched ($v_s \approx 5$ m/s)
Overquenched ($v_s \gtrsim 20$ m/s)

Ribbons (or flakes) of 30-50 μm thickness are thrown off the wheel surface

Melt-spun Nd-Fe-B: quenching rate

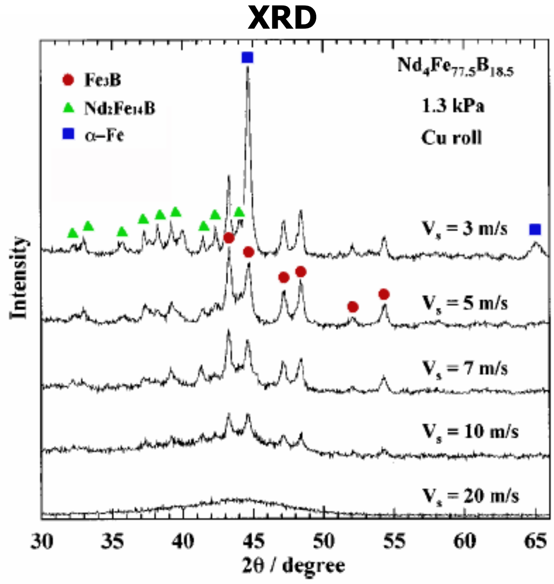

Kanekiyo et al., JAP 83 (1998) 6265.

Underquenched (very slow v_s)
Multidomain $Nd_2Fe_{14}B$
<D> = 100 nm...10 µm;
large α-Fe inclusions

Optimally quenched ($v_s \approx 5$ m/s)
$Nd_2Fe_{14}B$ grain size < 100 nm
+ soft magnetic α-Fe and Fe_3B

Overquenched ($v_s \approx 20$ m/s)
amorphous (Fe-rich alloys)
amorphous/nanocrystalline

Melt-spun Nd-Fe-B: quenching rate

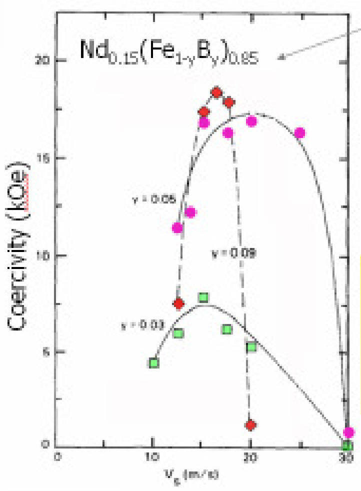

Croat et al.,1984

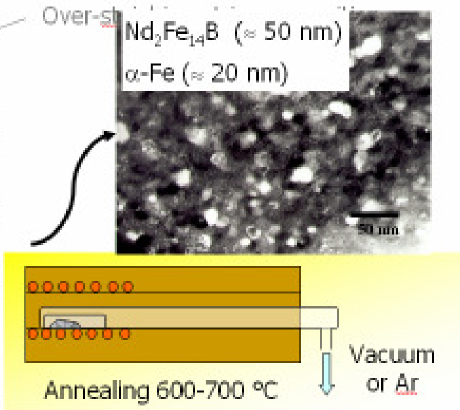

Overquenched
amorphous (Fe-rich alloys)
amorphous/nanocrystalline

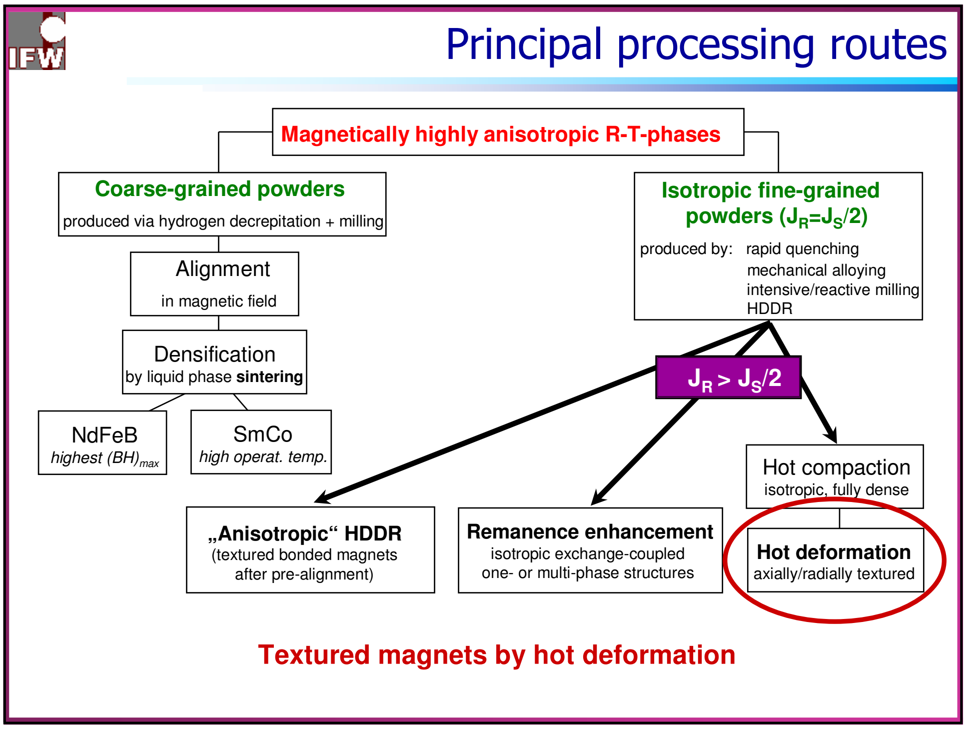
IFW
Principal processing routes
Magnetically highly anisotropic R-T-phases
Coarse-grained powders
produced via hydrogen decrepitation + milling
Alignment
in magnetic field
Densification
by liquid phase sintering
NdFeB
highest $(BH)_{max}$
SmCo
high operat. temp.
Isotropic fine-grained powders ($J_R=J_S/2$)
produced by: rapid quenching
mechanical alloying
intensive/reactive milling
HDDR
$J_R > J_S/2$
Hot compaction
isotropic, fully dense
„Anisotropic“ HDDR
(textured bonded magnets after pre-alignment)
Remanence enhancement
isotropic exchange-coupled one- or multi-phase structures
Hot deformation
axially/radially textured
Textured magnets by hot deformation

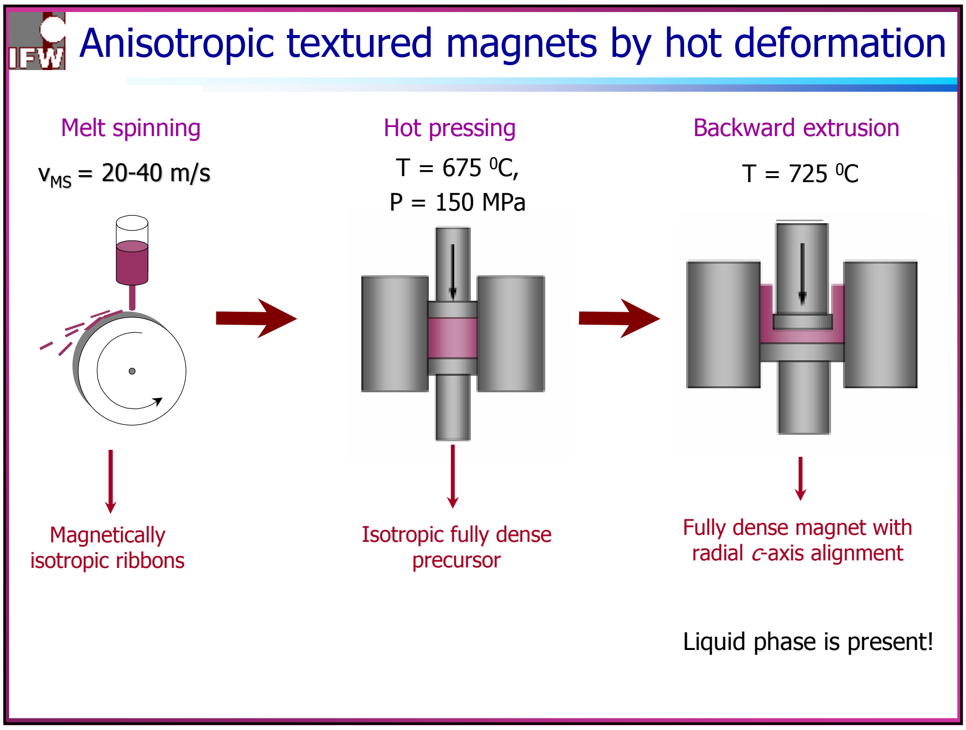
IFW
Anisotropic textured magnets by hot deformation
Melt spinning
v_{MS} = 20-40 m/s
Hot pressing
T = 675 ^{0}C,
P = 150 MPa
Backward extrusion
T = 725 ^{0}C
Magnetically isotropic ribbons
Isotropic fully dense precursor
Fully dense magnet with radial *c*-axis alignment
Liquid phase is present!

Texture in fine grained NdFeB magnets

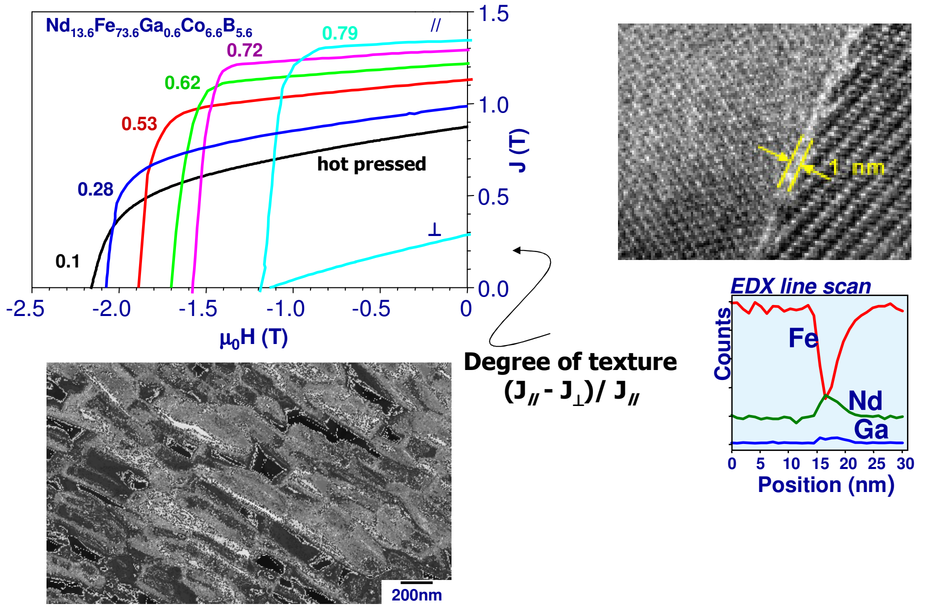

Texture in fine grained NdFeB magnets

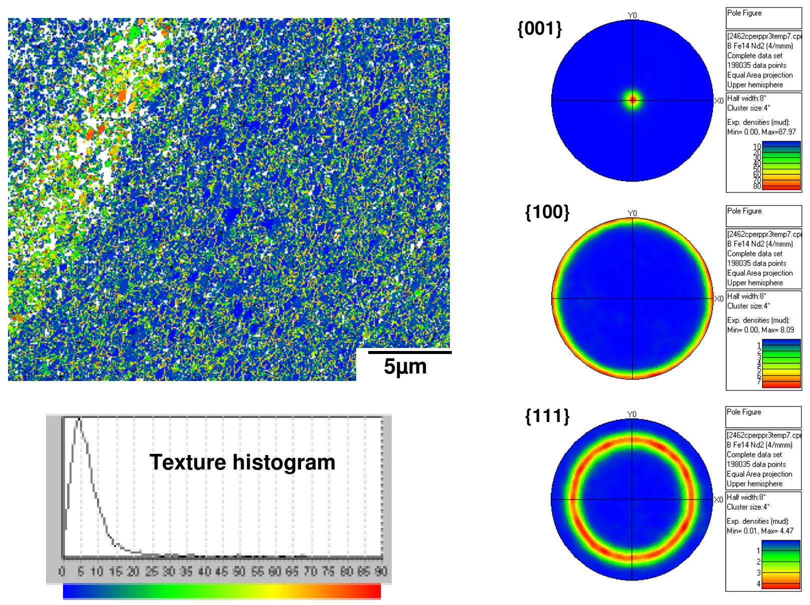

Principal processing routes

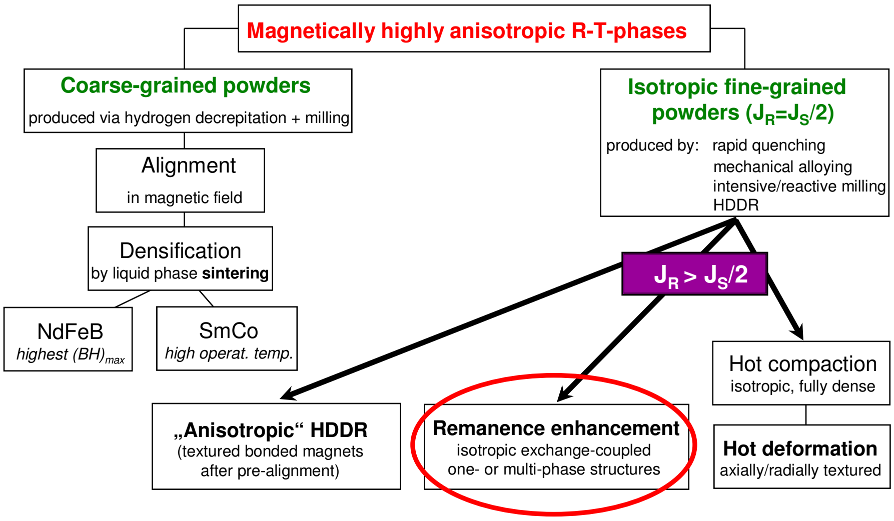

Isotropic remanence-enhanced magnets

O. Gutfleisch, J. Phys. D: Appl. Phys. **33** (2000) R157.

Fe-Pt alloys

Phase diagram and crystal structures

Magnetism of Fe-Pt

Phase formation in nanocrystalline Fe-Pt alloys

Structure and magnetic properties

Magnetisation reversal processes

Magnetic moments of ordered and partially ordered Fe-Pt

→ APL 89 (2006) 032506

Applications: thin films/nanoparticles

Data storage

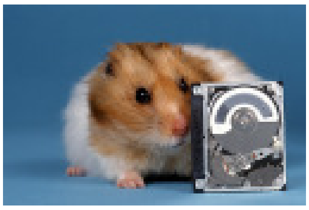

(Micro-drive IBM 1Go)

FePt self-organising media

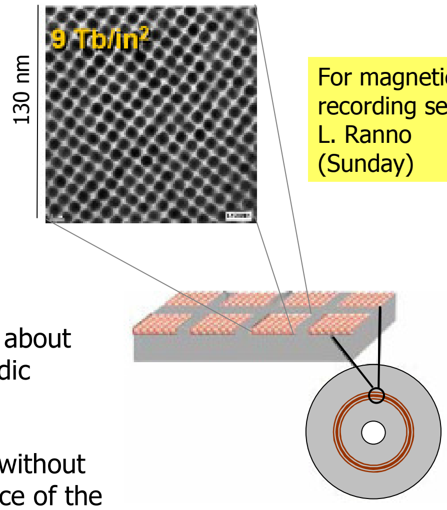

For magnetic recording see L. Ranno (Sunday)

Seagate Technology

Needs: monodisperse FePt particles about 4 nm in size self-assembled in periodic arrays over an extended area

Challenges: obtaining $L1_0$ structure without undesired agglomeration, coalescence of the particles and loss of periodicity

Applications: thick films/bulk

MEMS (magnetic MEMS)

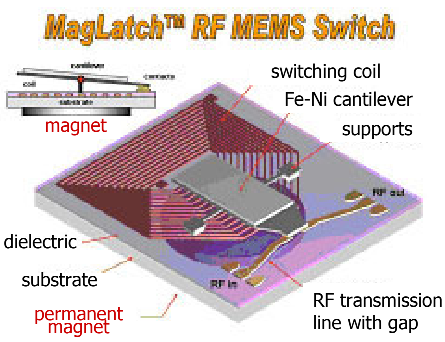

Motors, actuators, sensors, telecommunicaition, robotics…

Medical application

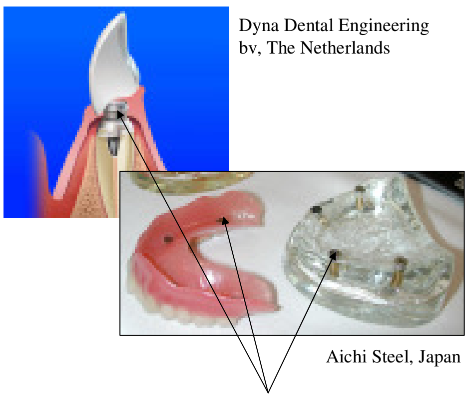

Dyna Dental Engineering bv, The Netherlands

Aichi Steel, Japan

permanent magnets

Fe-Pt phase diagram

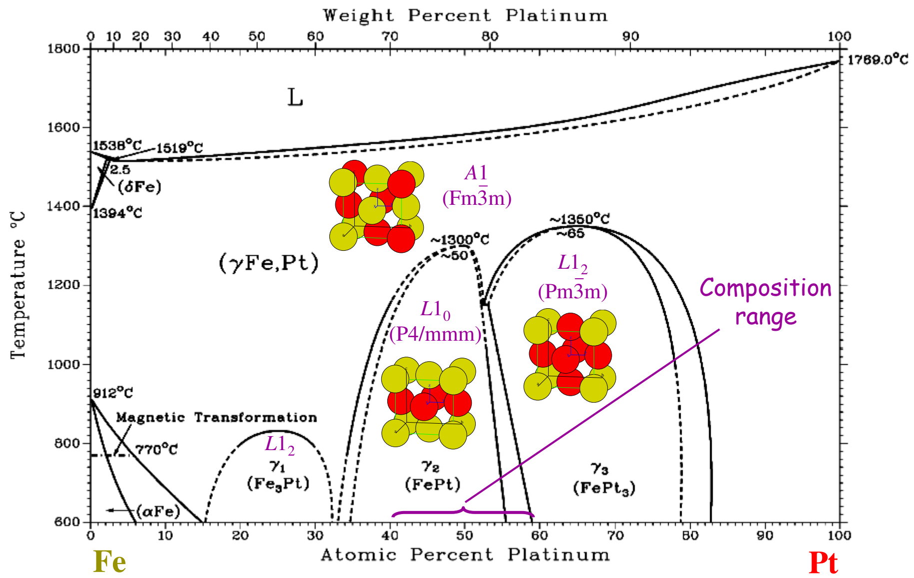

Magnetic moments

Spontaneously spin-split bands

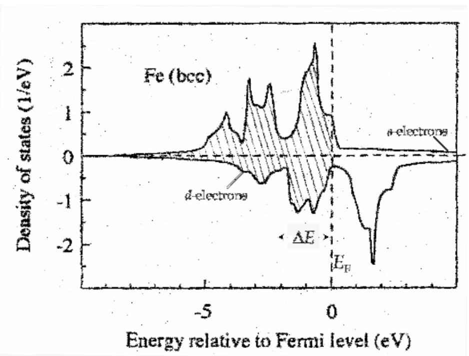

FePt – itinerant ferromagnet

Stoner criterion: $\mathbf{I \cdot N(E_F) > 1}$

- Strong exchange interaction I

  $I = \Delta E / \mu_s$

- Large density of states $N(E_F)$

Spin moment: $\mu_s = \mu_B (n_\uparrow - n_\downarrow) = -2\mu_B \langle S_z \rangle / \hbar$

Magnetic moments

Stoner criterion:
I·N(E_F) > 1

	Magnetic moment, μ_B μ_s	μ_l	μ_{tot}	SO coupling ξ, eV	I·N(E_F)
α-Fe	2.23	0.04	2.27	0.07	1.5-1.7
Pt	exchange-enhanced paramagnet			0.6	0.5-0.7

$$\chi = \frac{2\mu_0\mu_B^2 N(E_F)}{1 - I \cdot N(E_F)}$$

Pauli paramagnet

5d(Pt)-3d(Fe) hybridisation in FePt ⇒ enhanced Fe moment ≈ 2.8 μ_B
induced moment on Pt sites ≈ 0.4 μ_B

$$\mu_{tot}\ (\text{FePt}) = \mu_s + \mu_l \approx \mu_s$$

μ_l (symmetry + ξ)

Magnetocrystalline anisotropy (MCA)

SO interaction couples the isotropic μ_s to the crystal lattice ⇒ MCA

MCA in $L1_0$ FePt ⇒ large SO coupling (ξ) in Pt + 5*d*(Pt)-3*d*(Fe) hybridisation

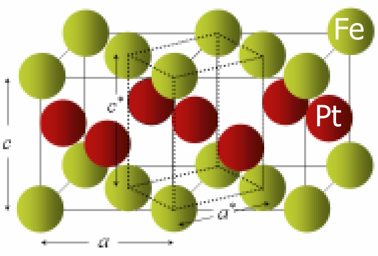

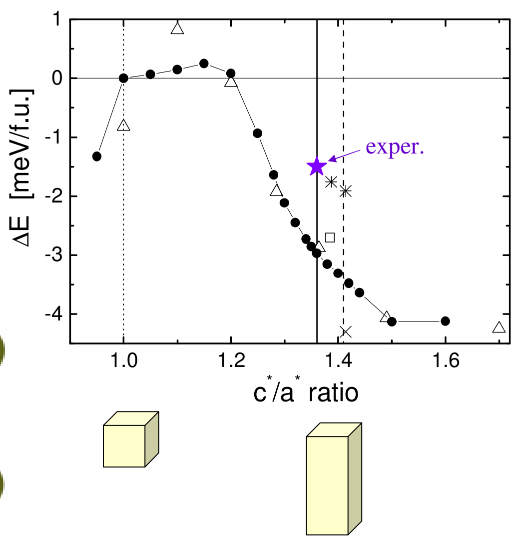

Lyubina et al., J. Phys.: Cond. Matter. 17 (2005) 4157

Magnetic properties of the Fe-Pt phases

Room temperature

	Fe_3Pt	FePt	$FePt_3$
Disordered	para	ferro	ferro
Ordered	ferro high M_s	ferro high K_1	para T> 160 K anti-ferro

Aim: Exchange coupled FePt/Fe_3Pt nanocomposite

Hard/soft nanocomposites

Intrinsic magn. properties /M_s, T_c, H_a/: interaction on the atomic scale

Extrinsic magn. properties /M_r, H_c, $(BH)_{max}$/: interplay structure ↔ intrinsic properties

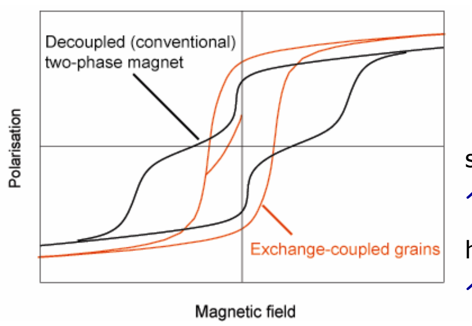

soft magnetic phase (α-Fe, Fe_3Pt...)

↑ $\mathbf{M_s}$

hard magnetic phase ($Nd_2Fe_{14}B$, $L1_0$ FePt...)

↑ $\mathbf{H_c}$

Exchange-coupling effective if

- grain size <D> sufficiently small (~ δ_W^{soft})
- phases suitably distributed

Mechanical ball milling at 77 K

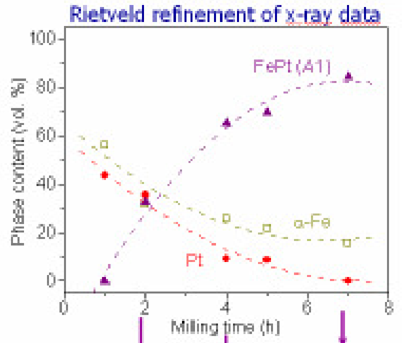

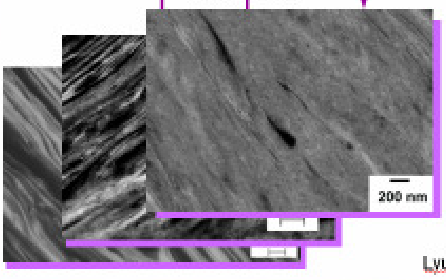

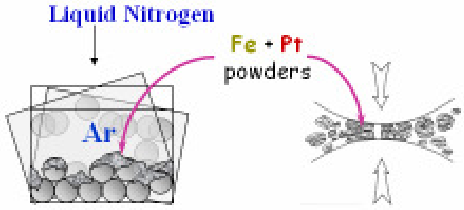

- a lamellar (multilayer-type) structure of Fe and Pt
- an intermediate structure: fine lamellae of Fe and Pt with *A*1 FePt at their interfaces
- homogeneous disordered *A*1 FePt

Lyubina et al., JAP 95 (2004) 7474; Scr. Mater. 53 (2005) 469

In-situ neutron diffraction: $Fe_{50}Pt_{50}$ (2 h milled)

α-Fe/Pt $\xrightarrow{\approx 300\ ^\circ C}$ $L1_0 + L1_2 \rightarrow L1_0$

Initial microstructure

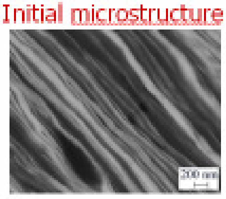

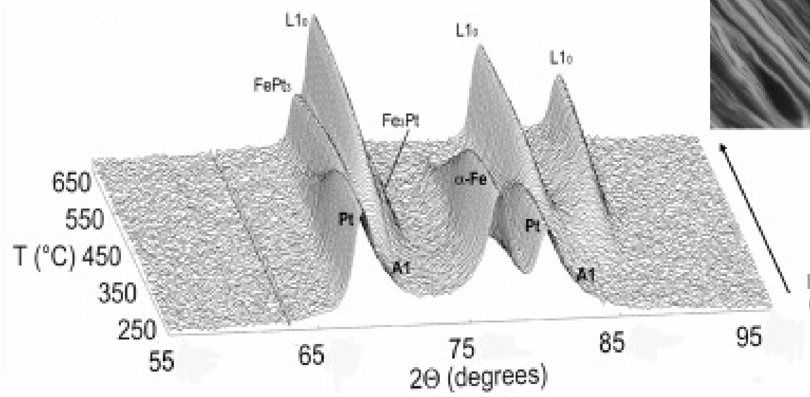

- Global equilibrium → $L1_0$
- $L1_0 + L1_2$ phases → a local equilibrium state provoked by the heterogeneous precursor material

Lyubina et al., JAP 100 (2006) 094308

In-situ neutron diffraction: $Fe_{50}Pt_{50}$ (4 h milled)

α-Fe/A1/Pt $\xrightarrow{\approx 300\ ^{\circ}C}$ $L1_0 + L1_2 \rightarrow L1_0$

Initial microstructure

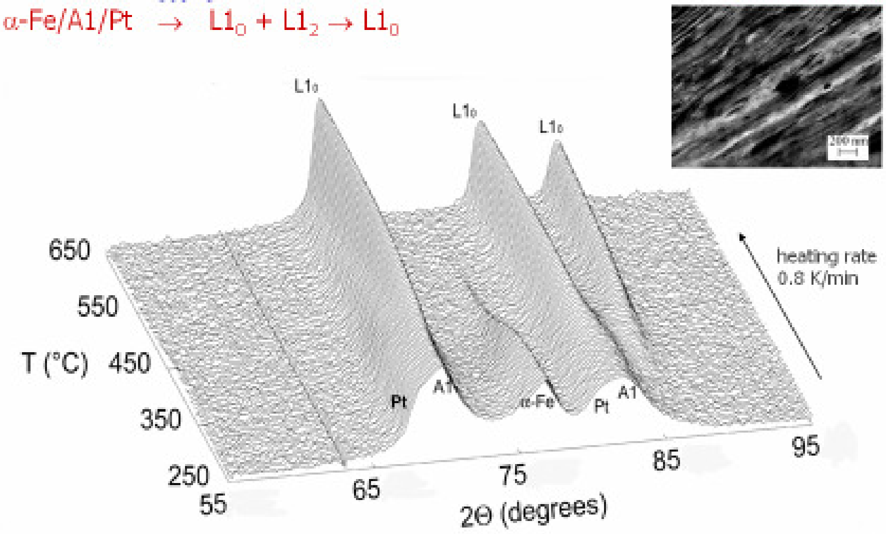

Lyubina et al., JAP 100 (2006) 094308

$Fe_{50}Pt_{50}$ (isothermal heat treatment)

2 h milled + 450°C/48 h

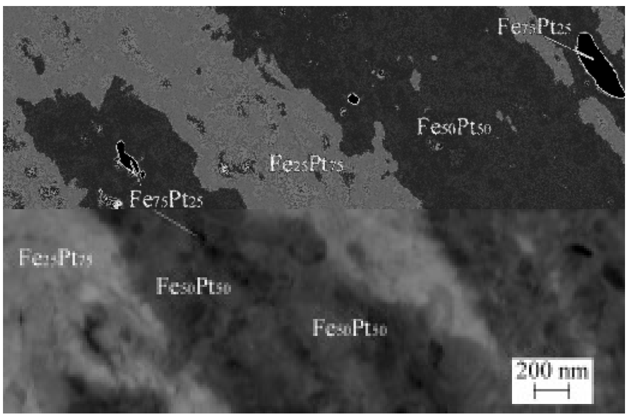

Lyubina et al., Scripta Materialia 53 (2005) 469.

- Microstructure preserves a lamellar character even after annealing
- The crystallites within the lamellae are substantially smaller than the lamellae thickness

$Fe_{50}Pt_{50}$: magnetic properties

Milling + 450 °C

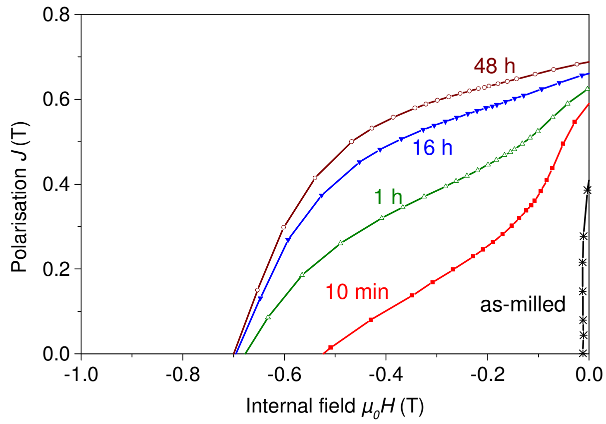

Lyubina et al., JAP 95 (2004) 7474.

- As-milled powders → soft magnetic behaviour
- A shoulder in the demagnetisation curves due to unreacted α-Fe (samples annealed for 10 min and 1 h)
- Optimum magnetic properties in $Fe_{50}Pt_{50}$ for 450 °C/48 h

$Fe_{100-x}Pt_x$: effect of composition

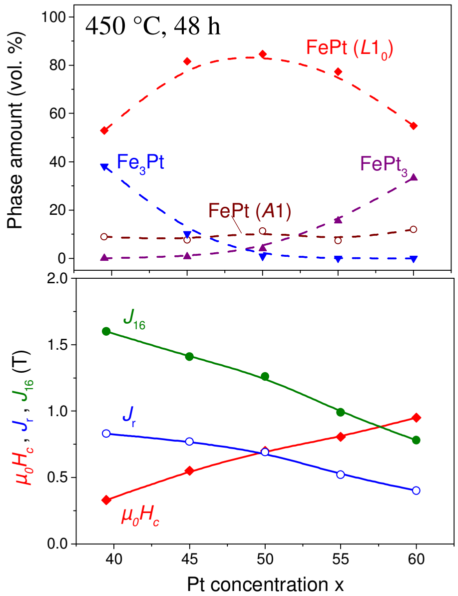

Heat treatment ⇒

well ordered $L1_0$ FePt (S = 0.91 – 0.98)

\+

$L1_2$ (Fe_3Pt or $FePt_3$)

H_c increases with x

up to x = 50 → due to $L1_0$ fraction increase, concurrent with Fe_3Pt amount reduction

for x > 50 → $FePt_3$ (paramagnetic at RT) decouples the grains within the lamellae of $L1_0$ FePt

Lyubina et al., JMMM 290-291 (2005) 547.

$Fe_{100-x}Pt_x$: exchange coupling

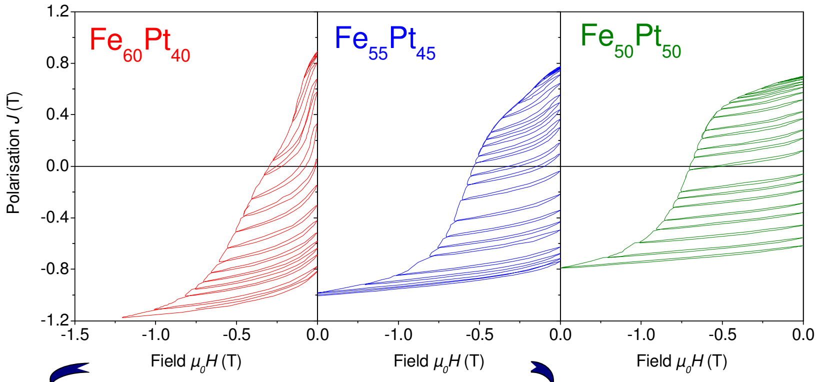

two-phase demagnetisation behaviour

- Fe-rich alloys: fairly high recoil permeability
  shoulder in the demagnetisation curves
- Weakly pronounced exchange-spring behaviour

JMMM 290-291 (2005) 547.

$Fe_{100-x}Pt_x$: exchange coupling

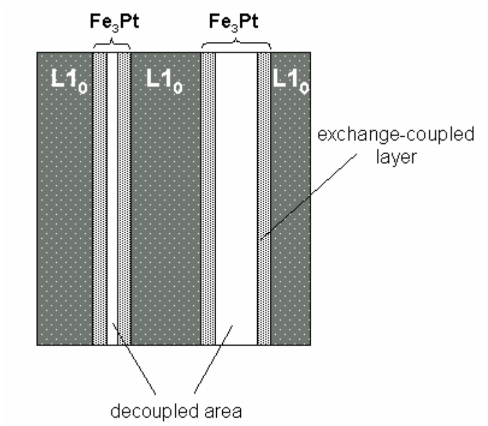

Grain size* of the phases is small enough for exchange-spring behaviour to be present:

FePt($L1_0$): <D> ≈ 30 nm

Fe_3Pt: <D> = 18-25 nm

Only a limited amount of the Fe_3Pt grains, the grains at the boundary of the $L1_0$ phase, can participate in exchange-coupling

* Obtained from the xrd line broadening after separation of size and strain effects

Exchange-spring FePt/Fe_3Pt

Nanoscale multilayer-type distribution of chemically highly ordered $L1_0$ FePt and Fe_3Pt

$Fe_{55}Pt_{45}$ (4 h milled + 450 °C/48 h)

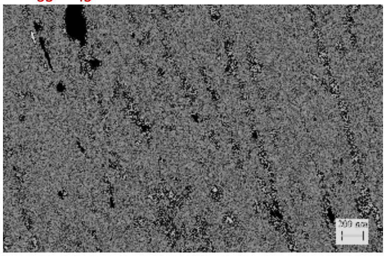

Exchange-spring behaviour

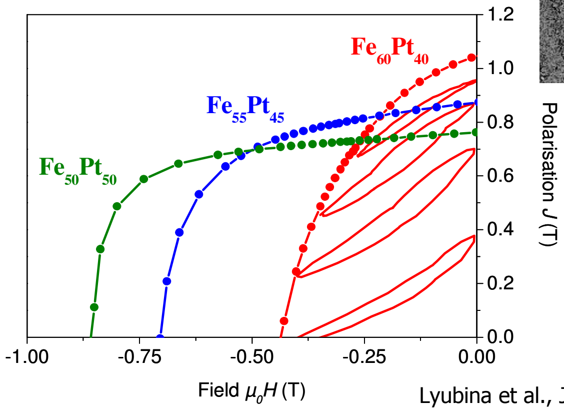

$Fe_{60}Pt_{40}$ $(BH)_{max}$ = 104 kJ/m³

$Fe_{55}Pt_{45}$ $(BH)_{max}$ = 121 kJ/m³

$Fe_{50}Pt_{50}$ $(BH)_{max}$ = 104 kJ/m³

Lyubina et al., J. Phys.: Cond. Matter. 17 (2005) 4157

Projections: permanent magnets

- Development and texturing of new nanocomposite systems
- Development of new non-equilibrium processing routes as well as texturing techniques
- Materials development requires all advanced characterisation techniques from electron microscopies, atom probe, synchrotron-based spectro–microscopies, neutron scattering, high resolution magnetic imaging to large-scale computational simulations

Projections: further progress in $(BH)_{max}$

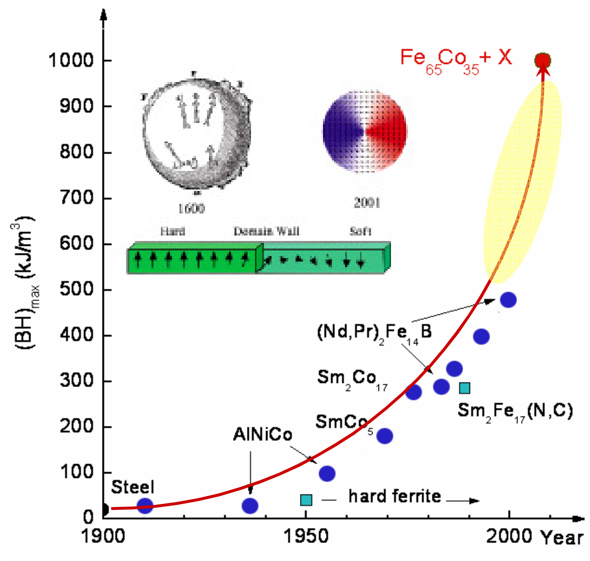

- Phase diagram simulation of quaternary, … systems
- Combinatorial techniques using material spreads

Magnetic and non- magnetic figures of merit

- magnetisation behaviour
- homogeneity of mag. prop.
- chemical stability
- thermal stability
- machineability
- net shape-processing
- geometry
- cost

Projections: magnetic MEMS

'Extreme' die-upset sheet shaped magnets

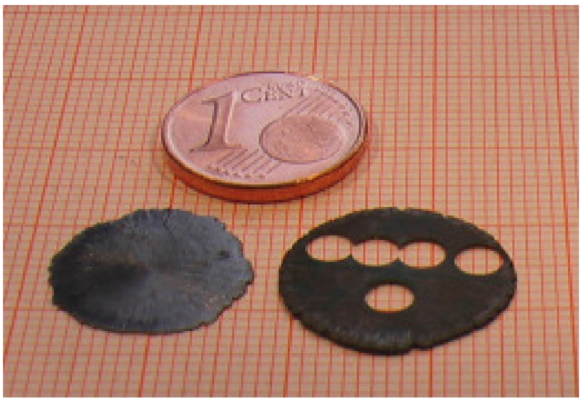

200 µm thick | 360 µm thick

D. Hinz et al., 18th Workshop on High Performance Magnets & their Applications, 2004, p.797.

Projections: magnetic MEMS

Demagnetisation curves

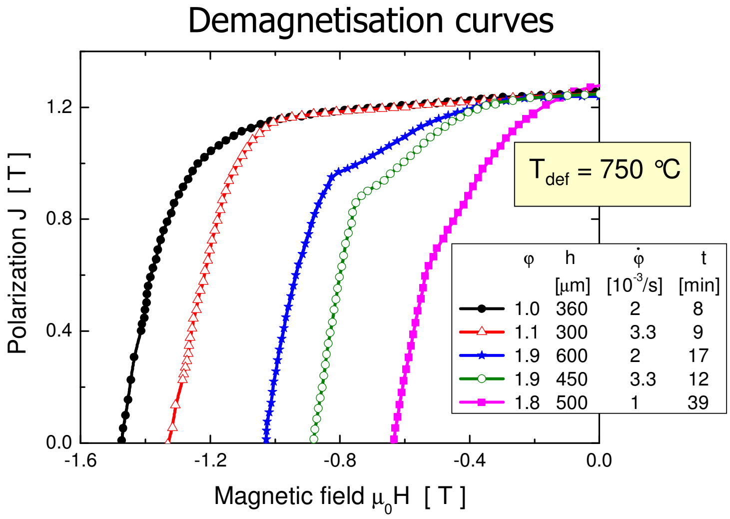

φ - strain, h - final thickness, φ̇ - strain rate, t – duration of die-upsetting

Projections: magnetic MEMS

Surface flux density distribution

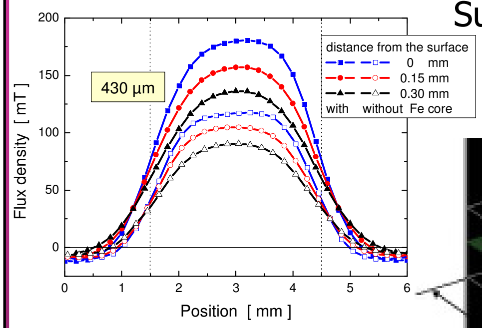

Line scan

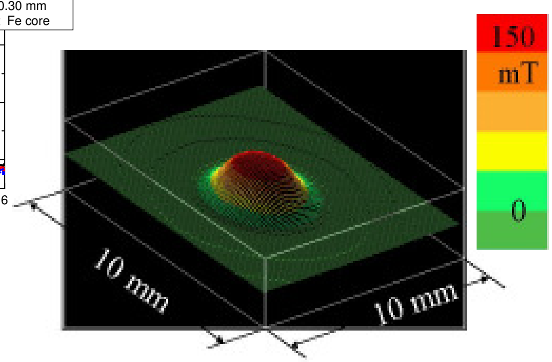

3D representation

D. Hinz et al., 18th Workshop on High Performance Magnets & their Applications, 2004, p.797.

Projections: magnetocaloric materials

Magnetocaloric effect (MCE)
→ emission or absorption of heat in a magnetic material in response to a changing magnetic field.

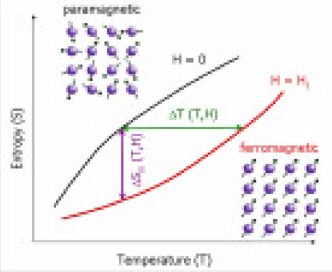

$$\Delta S_m = \int_0^H \left(\frac{\partial M}{\partial T}\right)_H dH$$

$$\Delta T_{ad} = -\int_0^H \frac{T}{C_{H,p}} \left(\frac{\partial M}{\partial T}\right)_{H,p} dH$$

high H
large $\left(\frac{\partial M}{\partial T}\right)_H$
small $C_{H,p}$
} large MCE

Magnetic refrigeration cycle

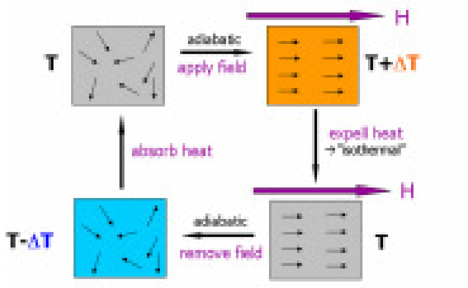

Advantages of magnetic cooling:

- ✓ environmentally friendly, no ozone depleting (CFCs) or hazardous chemicals (NH_3), no greenhouse gases
- ✓ higher energy efficiency
- ✓ easily scalable cooling power (mW to kW)
- ✓ mechanically simple – reduced noise

Problems / Requirements:

- large $(\partial M/\partial T)_{H,T}$, large ΔS at T_C, large field dependence of T_C
- large $\Delta T_{ad}/\Delta H$ driven by moderate magnetic fields (RPMs)
- small thermal and magnetic hysteresis
- material cost (e.g. Gd), non-toxic (e.g. As)
- high thermal and small electrical conductivity
- mechanical stability, high ductility